

# Polarized Multispectral Imaging for the Diagnosis of Skin Cancer

Laura Rey-Barroso<sup>1\*</sup>, Francisco J. Burgos-Fernández<sup>1</sup>, Santiago Royo<sup>1</sup>, Susana Puig<sup>2</sup>, Josep Malvehy<sup>2</sup>, Giovanni Pellacani<sup>3</sup>, Xana Delpueyo<sup>1</sup>, Sara Peña<sup>1</sup>, Fernando Díaz-Doutón<sup>1</sup> and Meritxell Vilaseca<sup>1</sup>

<sup>1</sup> Centre for Sensors, Instruments and Systems Development, Technical University of Catalonia; Terrassa, Spain

<sup>2</sup> Dermatology Department of the Hospital Clinic of Barcelona, IDIBAPS; Barcelona, Spain

<sup>3</sup> Università di Modena e Reggio Emilia; Modena, Italy

## Abstract

*The effective and non-invasive diagnosis of skin cancer is a hot topic in biophotonics since the current gold standard, a biopsy, is slow and costly. Non-invasive optical techniques such as polarization and multispectral imaging have arisen as powerful tools to overcome these constraints. The combination of these techniques provides a comprehensive characterization of skin chromophores including polarization, color and spectral features. Hence, in this work we propose a polarized multispectral imaging device that works from 414 nm to 995 nm and at 0°, 45° and 90° polarization configurations. Preliminary results performed over 20 nevi and 20 melanoma found statistically significant descriptors ( $p < 0.05$ ) that discriminated between these two lesion etiologies. A further analysis of more lesions is expected to contribute in reducing the false positives during the diagnosis process and, as a consequence, the number of necessary biopsies.*

## Introduction

The incidence of skin cancer increases every year so that its diagnosis and treatment is crucial. The World Health Organization estimates that 60.000 people die every year from skin cancer: 48.000 from melanoma, which is the most aggressive form, and 12.000 from other non-melanocytic skin cancers [1]. Visual inspection followed by dermoscopy is the classical approach to diagnose this disease. However, there is a relevant percentage of false positives and the only gold standard for the final diagnosis is to excise the lesion (biopsy) to undergo histological examination under a microscope. Dysplastic nevi, more commonly known as atypical moles, are benign lesions that often resemble melanoma. In the visual inspection process, they may feature different colors, appear asymmetrical or have odd borders. In addition, people with dysplastic nevi are at higher risk of developing melanoma, so most nevi are excised for prevention causing most of the false positive cases that imply high costs for the health insurance system and the patients' discomfort. This is why specialist are highly interested in distinguishing nevi and melanoma in a non-invasive way. For these reasons, several efforts have been put in detecting skin cancer quantitatively and non-invasively through optical and photonic tools such as multispectral imaging, which provides images through several spectral bands with high spatial resolution. Thus, it is possible to obtain pixel-wise spectral features of the skin lesion, which can then be used as a spectral signature since substances and structures inside might change – and thus, their absorbance and scattering features – when it becomes malignant. Besides, the texture of the lesion can also change, and thus the polarization state of the reflected light. However, most of the multispectral images are

acquired using an analyzer (two polarizers completely crossed, 90°) in order to diminish specular reflection from the skin surface. Usually, multispectral systems for skin analysis include spectral bands from 400 nm to 950 nm even though the infrared range up to 1613 nm have also been explored [2]. They use indirect illumination by means of Liquid Crystal Tunable Filters [3,4], filter wheels [5], fiber bundles [6] or direct illumination [7] by means of multiplexed light sources. The number of spectral bands used usually ranges from four to ten but in some studies, authors have implemented hyperspectral imaging with more than 100 channels [8]

Despite the fact that sensitivity and specificity obtained with the former multispectral imaging systems have reached values similar to those obtained by experienced dermatologists through dermoscopy, they have not yet superseded histological examination. In fact, it is still the clinical gold standard, providing diagnostic confirmation after surgical excision of the tumor. Commercial devices based on this approach, such as SIAscope<sup>®</sup> and MelaFind<sup>®</sup>, often present high values of sensitivity to distinguish melanoma from other benign lesions, but they retrieve low values of specificity.

On the other hand, it is known that polarization can carry additional information since it is a more general physical feature of light than intensity and orthogonal to wavelength [9]. The combination of multispectral imaging with the polarization states of light at different angles will represent a step forward the analysis of skin lesions [10, 11]. Therefore, in this work we propose the non-invasive assessment of skin lesions through a polarized multispectral (PMS) imaging system that includes an analyzer with 0°, 45° and 90° polarization configurations.

## Polarized Multispectral Imaging System

The developed PMS imaging system (Fig. 1a) is able of capturing reflectance and color features in the visible (VIS) and near infrared (NIR) ranges at three polarization configurations [7]. It consists of a DMK 23U445 CCD camera with 12-bit depth and 1280 x 960 pixels (The Imaging Source Europe GmbH). The lens coupled was a Cinegon 1.8/16 from Schneider-Kreuznach with spectral sensitivity from 400 nm to 1000 nm, which allowed a working distance of 40 mm and a field of view of 15 mm x 20 mm. Sequential multiplexed illumination is used by means of a ring of 32 LEDs (four per wavelength) with the following peak wavelengths: 414 nm, 447 nm, 477 nm, 524 nm, 671 nm, 735 nm, 890 nm, and 995 nm (Fig. 1b).

In addition, two polarizers working from 400 nm to 700 nm and with a 38% of transmission for unpolarized light were included; one is located in front of the LEDs (Fig. 1c) and the other in front of the lens. The later can be rotated with respect

to the former to acquire the spectral images at three different angles of polarization (Fig. 1d): 90° (polarizers are crossed), 45° and 0° (polarizers are parallel). When the polarizers are crossed, the specular reflection of the skin is removed as only light that is backscattered from deeper layers with changed polarization is allowed to pass. On the contrary, when they are parallel, the information obtained comes mostly from the first surface of the skin where the specular reflection takes place. It must be noted that specular reflection does not change the polarization of light. This effect is more obvious at shorter wavelengths as they are usually strongly reflected superficially by the skin. Since the polarizers work up to 700 nm, the three last spectral bands of the device (735 nm, 890 nm, and 995 nm) were not considered when computing polarization parameters.

A user friendly software based on C++ was developed, for controlling the synchronous firing of the LEDs and acquisition of the camera sensor. The different configurations of the polarizers are manually controlled, obtaining a spectral cube of five images per polarization configuration.

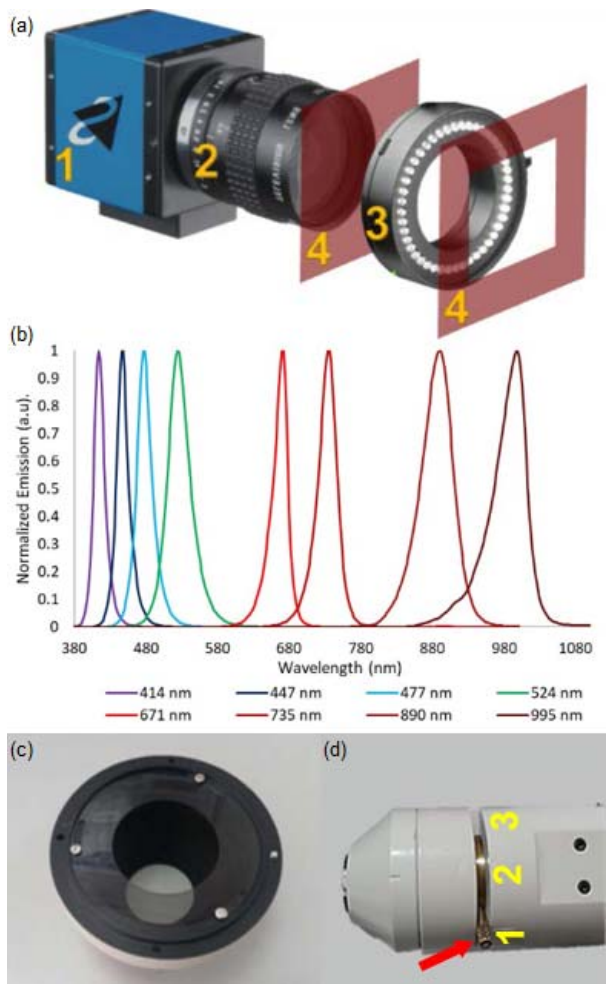


**Figure 1.** (a) Components of the developed PMS imaging system: 1. camera, 2. objective lens, 3. LED ring, 4. polarizers. Polarizer attached to the conus (b) Spectral emission of LEDs. and (c) top view of the system's head with (d) the lever that allows the variation of the angle of polarization: 1. 90°, 2. 45°, and 3. 0°.

## Clinical Study

The clinical measurements were carried out at the Hospital Clínic i Provincial de Barcelona (Spain) and the Università degli Studi di Modena e Reggio Emilia (Italy), within the framework of the European project DIAGNOPTICS ("Diagnosis of skin cancer using optics"). For this purpose, two identical multiphotonic platforms including the described multispectral system were installed at each location.

A total of 654 suspicious skin lesions from Caucasian individuals attending both hospitals were finally included in the study. Each lesion was considered suspicious unless it presented obvious clinical-dermoscopic features of benignity. The measurement area over the skin was cleaned and hair was carefully cut instead of shaved to avoid irritation. In this preliminary study, only 20 nevi and 20 melanomas were evaluated.

A metallic ring was glued to the patient's skin for the tip of the device to remain steady and parallel to the surface of the skin. All patients provided written informed consent before any examination and ethical committee approval was obtained. The study complied with the tenets of the 1975 Declaration of Helsinki (Tokyo revision, 2004). The lesions were diagnosed by dermatologists using a commercial dermoscope and the confocal laser scanning microscope VivaScope® 1500 from MAVIG GmbH. When malignancy was suspected, the lesion was excised and a histological analysis was carried out. From the total set of lesions, 94.8% (620) could be measured with the PMS imaging prototype; in the remaining 5.2% (34) the use of the metallic ring was impractical for the body area involved.

## Image Processing

The spectral images at five spectral bands from 414 nm to 671 nm and for 0°, 45° and 90° polarization configurations were obtained for each of the 620 available lesions. Figs. 2a and 2b show examples of the images obtained at polarizations of 0°, 45° and 90° for 414 nm, 524 nm and 671 nm for a nevus and a melanoma, respectively. From these raw images, it can be observed that specular reflections were removed at 90° but they affected remarkably the image of 0°. Depending on the type of skin and lesion, the intensity of the polarized reflected light may vary at the different wavelengths.

Fig. 2c shows the reflectance spectra of these two lesions at all wavelengths from 414 nm to 671 nm and for the three polarization configurations. The configuration where both lesions presented similar values was at 0°, in which specular reflections are more notorious. In spite of this, the largest differences between nevi and melanomas appeared for longer wavelengths for the three polarization states.

The state of polarization measured with the developed system is only partially linear since the total state of polarization could only be assessed by means of Stokes imaging [12]. According to the literature, partial linearly polarized light is described by three parameters: the orientation of linear polarization, known as the phase or simply angle of polarization  $\theta$  (Eq. 1), varying within the range  $[0^\circ, 180^\circ]$ ; the intensity of the image (Eq. 2) [9], which is calculated as the sum of the polarization images at 0° and 90°; the relative proportion of linear polarization, known as the degree of polarization, varying between 0 and 1, from unpolarized to completely linearly polarized light; nevertheless, it is often replaced by the orthogonal state contrast, OSC, which is more straightforward (Eq. 3) [13]. The angle of polarization,

intensity, and the orthogonal state contrast determine the state of partial linear polarization.

$$\theta = \frac{1}{2} \tan^{-1} \left( \frac{I_0 + I_{90} - 2I_{45}}{I_{90} - I_0} \right) + 90 \quad (1)$$

if  $(I_{90} < I_0)$  [if  $(I_{45} < I_0)$   $\theta = \theta + 90$  else  $\theta = \theta - 90$ ]

$$Intensity = I_0 + I_{90} \quad (2)$$

$$OSC = \frac{I_{90} - I_0}{(I_{90} + I_0)} \quad (3)$$

where  $I_0$ ,  $I_{45}$  and  $I_{90}$  correspond to the digital level of the images at  $0^\circ$ ,  $45^\circ$  and  $90^\circ$  polarization configurations.

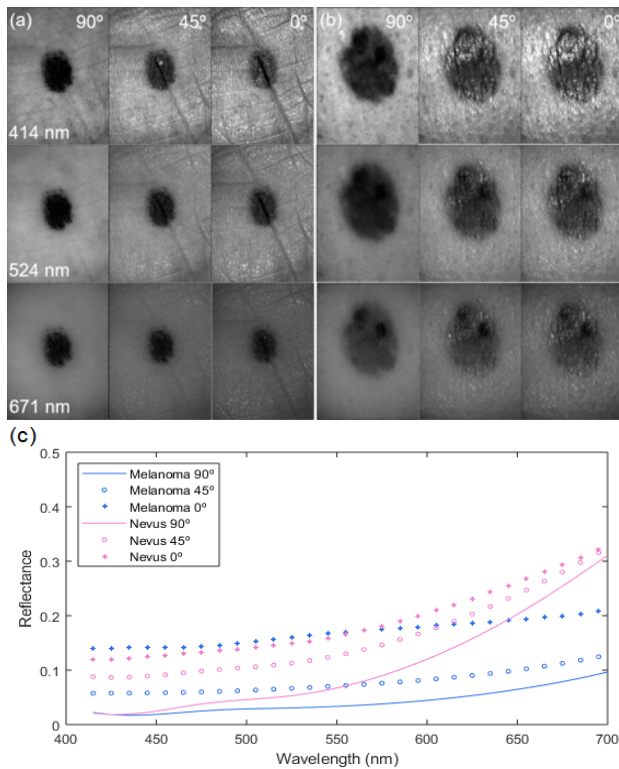


**Figure 2.** PMS images of a nevus (a) and a melanoma (b) at  $90^\circ$ ,  $45^\circ$ ,  $0^\circ$  for 414 nm, 524 nm and 671 nm. (c) Average spectral reflectance curves of a nevus and a melanoma at the three polarization configurations.

These three polarization parameters were computed for all images considered including melanomas and nevi. Afterwards, each lesion was manually segmented from the surrounding healthy skin in order to isolate the polarization information. This was done within a graphic user interface in which the lesion image could be opened and manually segmented. A binary mask was obtained from the segmentation and this was multiplied by the whole stack of polarization images, in order to remain with just the gray values from the lesion. From the segmented images, first order statistical descriptors were calculated such as the mean, standard deviation, maximum, minimum, and parameters coming from the image histogram as the energy, entropy and skewness [14]. These first order statistics were compared between the two etiologies to evaluate statistically significant differences using SPSS® statistics V23.0 (IBM Corp.). Comparisons were considered to be statistically

significant for  $p$ -values below 0.05. The Kolmogorov-Smirnov (KS) test was used to evaluate the normal distribution of all parameters and the t-Student (TS) test was used to compare normally distributed parameters amongst groups. For non-parametric variables, the Mann-Whitney U (MWU) test was used instead.

## Results

Lesions presented in Fig. 2 are also shown in the subsequent images after the corresponding processing. Fig. 3 contains the images in terms of the angle of polarization vs. wavelength. While the nevus can be distinguished at all wavelengths, especially at 414 nm and 671 nm, the melanoma is hardly visible. Only at 671 nm, the melanoma is more contrasted.

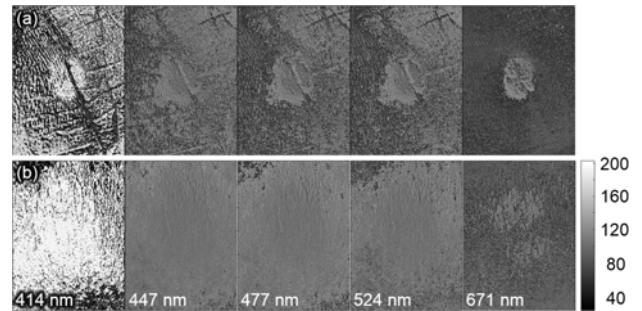


**Figure 3.** Angle of polarization images from 414 nm to 671 nm for a nevus (a) and a melanoma (b).

The intensity images vs. wavelength are shown in Fig. 4. For longer wavelengths, the specular component decreases, as light penetrates deeper into the tissue and is more scattered while the intensity increases particularly at 671 nm in the case of the melanoma.

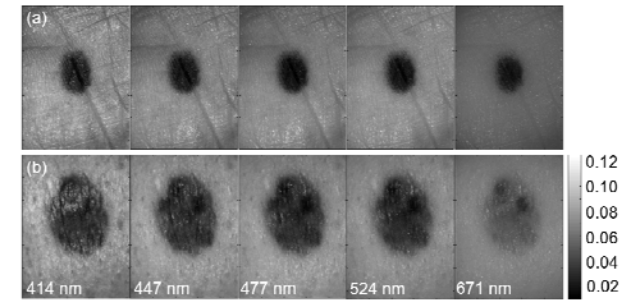


**Figure 4.** Intensity images from 414 nm to 671 nm for a nevus (a) and a melanoma (b).

The images in terms of orthogonal state contrast at each wavelength for a nevi and a melanoma are shown in Fig. 5. It retrieved higher values at shorter spectral bands, which means that the partial polarization of reflected light is greater at these wavelengths.

The KS test found statistical descriptors with normal and non-normal distribution and thus, the MWU and TS tests were applied accordingly to report statistically significant differences between nevi and melanoma. The angle of polarization at 414 nm showed differences with  $p < 0.001$ ; the rest of parameters included in Table 1 exhibited also significant differences but with  $p < 0.05$ .

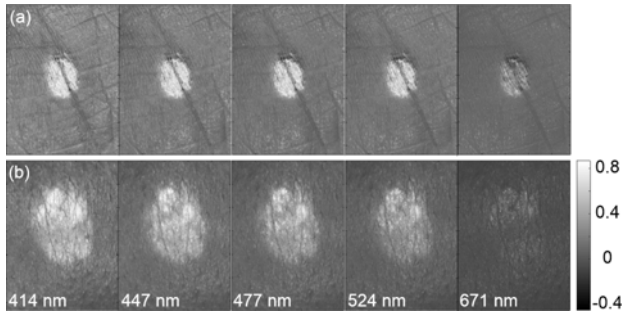


**Figure 5.** Orthogonal state contrast images from 414 nm to 671 nm for a nevus (a) and a melanoma (b).

**Table 1. Statistical Descriptors with Statistically Significant differences among groups ( $p < 0.05$ , KW and TS test): mean, standard deviation (SD), skewness ( $\mu_3$ ), minimum (Min.) and maximum (Max.) for the angle of polarization ( $\theta$ ), the intensity ( $I$ ) and the orthogonal state contrast (OSC). For each descriptor, the following values are given: mean ( $\pm$  standard deviation) and the minimum and maximum values (in parenthesis).**

Statistical descriptors	Nevus	Melanoma
$\theta$ Mean 414 nm ( $p < 0.001$ )	152.56 $\pm$ 15.65 (123.51, 179.61)	167.59 $\pm$ 9.57 (154.94, 187.88)
$\theta$ SD 414 nm ( $p = 0.001$ )	50.56 $\pm$ 18.02 (19.63, 70.30)	30.24 $\pm$ 16.44 (5.36, 61.09)
$\theta$ SD 447 nm ( $p = 0.002$ )	15.88 $\pm$ 4.44 (7.58, 25.59)	11.66 $\pm$ 3.66 (4.91, 17.22)
$\theta$ SD 671 nm ( $p = 0.004$ )	27.98 $\pm$ 5.62 (12.46, 34.80)	23.58 $\pm$ 2.99 (18.60, 28.36)
$I$ SD 524 nm ( $p = 0.012$ )	0.011 $\pm$ 0.002 (0.007, 0.013)	0.013 $\pm$ 0.002 (0.008, 0.017)
$\theta$ SD 477 nm ( $p = 0.014$ )	16.66 $\pm$ 4.61 (8.32, 25.96)	13.10 $\pm$ 4.16 (5.24, 20.77)
$I$ Min. 671 nm ( $p = 0.024$ )	0.024 $\pm$ 0.011 (0.006, 0.040)	0.017 $\pm$ 0.009 (0.006, 0.039)
$\theta \mu_3 \times 10^4$ 414 nm ( $p = 0.028$ )	-20.55 $\pm$ 10.25 (-33.41, -51.42)	-12.89 $\pm$ 12.56 (-36.58, -3.77)
OSC Max. 671 nm ( $p = 0.033$ )	0.53 $\pm$ 0.17 (0.19, 0.86)	0.66 $\pm$ 0.20 (0.18, 0.93)

As an example, Fig. 6 contains scatter plots of the mean of the angle of polarization at 414 nm and the standard deviation of the angle of polarization at 671 nm. At 414 nm, melanomas showed higher mean values of the angle of polarization, while values from nevi remained below. The scatter plot for the standard deviation at 671 nm revealed the opposite behavior with melanomas, which present lower values.

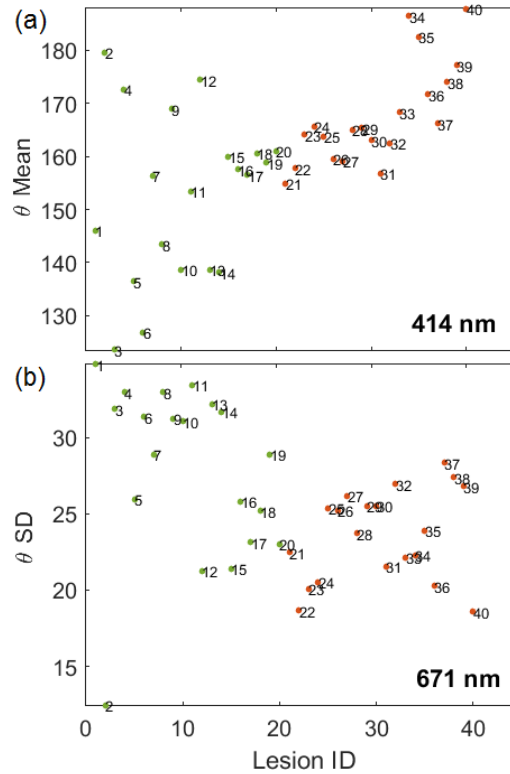


**Figure 6.** Statistical descriptors where green points are nevi and orange points are melanomas. Mean of the angle of polarization at 414 nm with  $p < 0.001$  (a), and standard deviation of the angle of polarization at 671 nm with  $p < 0.05$  (b).

## Conclusions

In this work, a polarized multispectral imaging system is used for the improvement of the diagnosis of skin cancer, especially to discriminate between melanomas and nevi. PMS images showed qualitative differences among these types of lesions that were quantified through the angle of polarization, intensity and orthogonal state contrast. The use of first order statistical descriptors and the posterior statistical analysis revealed statistically significant differences between melanomas and nevi especially at short wavelength, 414 nm and 447 nm, and for the mean and standard deviation of the angle of polarization.

Ongoing work is focused on processing the whole set of skin lesions to include them in the statistical analysis. Additionally, we are also considering the use of supervised machine learning algorithms as alternative method to classify skin lesions, since a larger dataset will provide greater robustness to this analysis than the preliminary reduced subset.

## References

- [1] World Health Organization. Available online: <https://www.who.int/en/> (accessed on 25 May 2018).
- [2] L. Rey-Barroso, F. J. Burgos-Fernández, X. Delpueyo, M. Ares, S. Royo, J. Malvehy, S. Puig, M. Vilaseca, "Visible and Extended Near-Infrared Multispectral Imaging for Skin Cancer Diagnosis" *Sensors*, 18 (2018)
- [3] I. Kuzmina, I. Diebele, D. Jakovels, J. Spigulis, L. Valeine, J. Kapostinsh, A. Berzina, "Towards noncontact skin melanoma selection by multispectral imaging analysis" *J. Biomed. Opt.*, 16 (2011)

- [4] A. Bekina, E. Lihacova, R. Uldis, J. Zaharans, A. Derjabo, J. Spigulis, "Multispectral Assessment of Skin Malformations Using a Modified Video-Microscope" *Lat. J. Phys. Tech. Sci.*, 49, 112 (2012)
- [5] R. Jolivot, Y. Benezeth, F. Marzani, "Skin parameter map retrieval from a dedicated multispectral imaging system applied to dermatology/cosmetology" *Int. J. Biomed. Imaging*, 2013 (2013)
- [6] S. Tomatis, A. Bono, C. Bartoli, M. Carrara, M. Lualdi, G. Tragni, R. Marchesini, "Automated melanoma detection: multispectral imaging and neural network approach for classification" *J. Med. Phys.*, 30, (2003)
- [7] X. Delpueyo, M. Vilaseca, S. Royo, M. Ares, L. Rey-Barroso, F. Sanabria, S. Puig, J. Malvey, G. Pellacani, J. Vázquez, G. Solomita, T. Bosch, "Multispectral imaging system based on light emitting diodes for the detection of melanomas and basal cell carcinomas: a pilot study" *J. Biomed. Optics. and Technol.*, 22, 65006 (2017)
- [8] T. Nagaoka, Y. Kiyohara, H. Koga, A. Nakamura, T. Saida, T. Sota, "Modification of a melanoma discrimination index derived from hyperspectral data: a clinical trial conducted in 2 centers between March 2011 and December 2013" *Skin Res Technol.*, 21 (2015).
- [9] L. B. Wolff, "Polarization vision: a new sensory approach to image understanding" *Image Vision Comput.*, 15 (1997)
- [10] F. Vasefi, N. MacKinnon, R.B. Saager, A.J. Durkin, R. Chave, E. H. Lindsley, D. L. Farkas, "Polarization-Sensitive Hyperspectral Imaging in vivo: A Multimode Dermoscope for Skin Analysis" *Nature Sci. Repts.*, 4, 4924 (2014)
- [11] P. Ghassemi, T. E. Travis, L. T. Moffatt, J. W. Shupp, J. C. Ramella-Roman, "A polarized multispectral imaging system for quantitative assessment of hypertrophic scars" *Biomed. Opt. Express*, 5, 10 (2014)
- [12] J. Dupont, M. Boffety and F. Goudail, "Precision of polarimetric orthogonal state contrast estimation in coherent images corrupted by speckle, Poisson, and additive noise" *JOSA A.*, 35, 6 (2018)
- [13] D. L. Andrews, *Instrumentation in Photonics, Volume 4: Biomedical Photonics, Spectroscopy, and Microscopy* (John Wiley & Sons, Hoboken, NJ, 2015) pg. 279.
- [14] G. Ritter and J. Wilson, *Image Features and Descriptors in Handbook of Computer Vision Algorithms in Image Algebra*, (CRC Press, Boca Raton, FL, 2000)